Empirical measurement of MEMS stroke saturation, with implications for woofer-tweeter architectures

Katie M. Morzinski [*a,b], Bruce A. Macintosh [a,b,c], Daren Dillon [a,b], Don Gavel [a,b], Dave Palmer [a,c], Andrew Norton [a,b]

[a] National Science Foundation Center for Adaptive Optics

[b] UCO/Lick Observatory and the Laboratory for Adaptive Optics, University of California, 1156 High St., Santa Cruz, CA 95064, USA

[c] Lawrence Livermore National Laboratory, 7000 East Ave., Livermore, CA 94550, USA

ABSTRACT

The Gemini Planet Imager (GPI) is currently in production for the Gemini Telescope in Chile. This instrument will directly image young jovian exoplanets, aided by a micro-electrical mechanical systems (MEMS) deformable mirror (DM). Boston Micromachines MEMS mirrors operate thousands of actuators to provide a well-sampled correction at high spatial frequencies. However, because MEMS stroke alone is insufficient to fully correct the atmosphere in the near-IR on an 8-meter telescope, a dual-mirror system is planned for GPI: The MEMS is used as a "tweeter" to correct the higher spatial frequencies while a separate "woofer" DM will be used to correct the lower frequencies. During operation at GPI, any saturated actuators would scatter starlight into the dark hole instead of allowing it to be removed coronagraphically; thus, stroke saturation on the MEMS is tolerated only at the 5-sigma level. In the Laboratory for Adaptive Optics, we test the ability of the MEMS to counter atmospheric turbulence. The MEMS shape is set to random iterations of woofer-corrected Kolmogorov phase screens with varying woofer sizes. We find that, for $r_0 = 10$ cm, saturation decreases from several percent to a few tenths of a percent ($\sim$3-sigma) when using a 100cm-pitch woofer. The MEMS we tested has 0.2 μm inter-actuator stroke for a 200V-range. Nonetheless, saturation (when it occurs) appears to be due to low-order peak-to-valley stroke even in the woofer-corrected case. Gemini characteristically has $r_0 = 15$ cm, so future work includes extrapolating to find where the 5-sigma saturation level occurs.

Keywords: MEMS; deformable mirror; stroke; extreme adaptive optics; woofer-tweeter

1. INTRODUCTION

The discovery of myriad extrasolar planets, including many with superjovian masses yet submercurial orbits, astonished and challenged astronomers to understand these exotic worlds.[1] Current exoplanet detection techniques include pulsar timing,[2] radial velocity measurements,[3] transit photometry,[4,5] and gravitational microlensing.[6] The Gemini Planet Imager (GPI) will add direct imaging to this list, which will increase not only the statistical counts of exoplanets while probing a complementary semimajor-axis space, but will also contribute valuable physical data to the field including mass, radius, temperature, and surface gravity of these objects.[7–9] This ambitious "extreme" adaptive optical (ExAO) instrument is under production for the Gemini South Telescope in Chile in late 2010. Through use of a high-order AO system, a specialized coronagraph, a unique calibration interferometer, and an integral-field spectrograph, GPI will be able to detect near-infrared photons from young jovian exoplanets 15 magnitudes fainter than their host star at separations of 0.2-1 arcsecond.

As a cutting-edge instrument, GPI plans to make use of some unconventional technologies, including the use of a non-traditional deformable mirror (DM) called a micro-electrical mechanical systems (MEMS) device. Boston Micromachines Corporation's MEMS DMs are manufactured in batch surface micromachining processes similar to silicon computer chips and are therefore compact with thousands of actuators.[10] Using these thousands of degrees of freedom to well-sample the wavefront, the MEMS enables the high-order correction required for

[*]Contact: ktmorz@ucolick.org; tel +1 831 459-1949; fax +1 831 459-5265

ExAO. However, with a continuous facesheet and given the physically small pitch (400 μm) of the MEMS actuators, a limited stroke can be achieved. The MEMS device at GPI will have 4.0 μm peak-to-valley and 1.3 μm inter-actuator stroke. Because correcting the wavefront errors for GPI across an 8m pupil requires more stroke than this, we plan to use what is termed a "woofer-tweeter" architecture. The MEMS DM is the "tweeter" which corrects the high-spatial-frequency aberrations that, in accordance with the Kolmogorov power law, have lower amplitude and therefore require less stroke. A separate "woofer" DM will correct the low-spatial-frequency aberrations that have higher amplitude and thus require more stroke.[11]

Choice of the appropriate woofer DM can mitigate stroke limitations of the MEMS DM. Stroke saturation occurs when a particular actuator is unable to move to the desired height due to insufficient stroke. During operation at GPI, any saturated actuators would scatter starlight into the dark hole (the region normally controlled by the AO system) instead of allowing it to be removed coronagraphically; thus, stroke saturation on the MEMS is tolerated only at the 5-sigma level. We use the ExAO testbed at the University of California at Santa Cruz's Laboratory for Adaptive Optics (LAO) to test the ability of the MEMS to counter atmospheric turbulence. The purpose of this study is to determine whether MEMS stroke saturation might be problematic for GPI.

2. BACKGROUND

2.1. Gemini Planet Imager system layout

The serial arrangement of the MEMS and woofer DMs in GPI will be as shown in Figure 1. There is also a third wavefront corrector: the tip/tilt stage, upon which the woofer is mounted. The AO system receives the light from the telescope and corrects the dynamic wavefront aberrations at up to 2500 Hz. The calibration system operates more slowly than the AO system but is more precise and uses interferometry to correct the non-common-path and the static wavefront aberrations. The net result is residual in-band wavefront error of order 1 nm rms. Flattening the wavefront so well is necessary for the apodized-pupil Lyot coronagraph to be able to best suppress the light from the central star. Finally, the integral-field spectrograph (IFS) obtains a spectrum of the target at each point across the image. The role of the MEMS DM is essential in providing the high-order correction GPI requires.

2.2. MEMS deformable mirrors at the Laboratory for Adaptive Optics

Through a development contract as well as some direct purchasing from Boston Micromachines Corporation, the LAO has studied and characterized two 144-actuator MEMS DMs, about ten 1024-actuator MEMS devices, and one 4096-actuator MEMS with a range of tests, including yield, dead-actuator zoology, hysteresis, stability, stroke, wavefront-flattening, coronagraphy, and open-loop control.[12–21] Figure 2 shows two of our MEMS devices at the LAO: one 1024-actuator DM and the new 4096-actuator DM, a prototype for the GPI MEMS. The stroke-saturation experiments for GPI were done with another 1024-actuator DM.

2.3. Stroke saturation

Stroke defines the maximum amplitude that can be corrected by a wavefront corrector (DM), and can be described in terms of inter-actutator stroke or peak-to-valley stroke. Saturation occurs when an actuator lacks the stroke necessary to correct part of a wavefront. Saturation can be at high or low spatial frequencies.

If actuators saturate under operation at GPI, the wavefront will not be well-corrected and light will scatter off the saturated actuators into the dark hole that is normalled carved out by the coronagraph. See Figure 3 for a pedagogical illustration of the effects of stroke saturation on the dark hole.

2.4. Preliminary stroke tests

Before studying MEMS stroke capabilities in terms of Kolmogorov atmospheres, we measured stroke as a function of spatial frequency.[18] One-dimensional striped sinusoids were applied to the MEMS, with the number of cycles across the MEMS being varied from 1 to 16. The resulting stroke-versus-spatial-frequency plots are shown in Figure 4 for two devices and at two different voltage ranges. See Morzinski *et al.*[18] for more detail.

Inter-actuator stroke is the difference between the height of two neighboring actuators when the actuators are sent to the opposite ends of the voltage range. With our MEMS devices in the LAO, we operate at either 160V
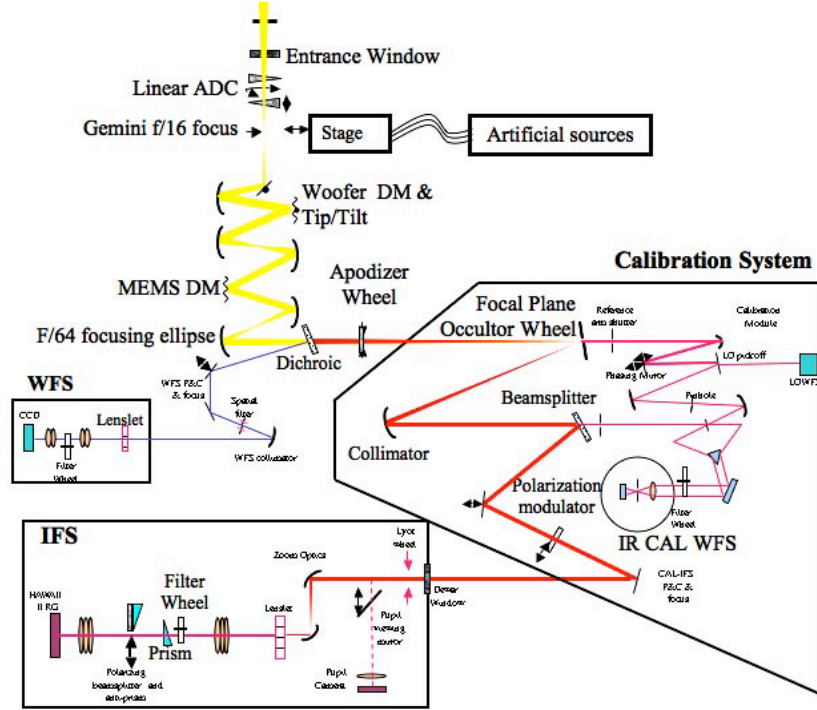
Figure 1. Sketch of the GPI system layout. The AO system is at the upper left with the yellow beam. There are three wavefront-correctors in the AO system: A woofer, a tip-tilt stage (physically supporting the woofer), and a tweeter (the MEMS).

MEMS Device Designation	Actuator Count	Pitch / μm	Max Volt Applied	Peak-to-valley stroke / μm surface	Inter-actuator stroke / μm surface
W10#X	1024	340	160	1.0	0.2
W107#X	1024	340	200	1.5	0.2
W95#39	1024	400	200	3.1	1.0
4kEng#1	4096	400	225	3.4	1.2
Predicted, Base GPI 4k	*4096*	*400*	*260*	*4.0*	*1.3*

Table 1. Table of MEMS stroke measured in the preliminary experiments for different MEMS devices and voltage ranges.

or 200V maximum. Therefore, the inter-actuator stroke is measured with one actuator at 0V and its neighbor at either 160V or 200V. Peak-to-valley stroke is the difference between the maximum and minimum heighths of the device, when different sections of the MEMS are set to the lowest and the highest voltage, respectively. Table 1 shows these measurements, which is redundant to the previous two figures for the two devices that had the entire range of spatial frequencies measured.

These preliminary experiments to understand the MEMS stroke showed that stroke is a rougly linear function of spatial frequency and that lower spatial frequencies have more stroke. The Kolmogorov power law has a similar qualitative form: a linear relation (between the inner and outer scales) that requires more stroke at the lower spatial frequencies. The question, however, is to determine where these two curves overlap, or the interplay between them. If Kolmogorov atmospheres have more power at the higher spatial frequencies than the MEMS has stroke, then stroke saturation could be a problem. Our GPI simulations do not indicate this to be true, but it is interesting to verify this with empirical laboratory tests.[22] Therefore, it remained to augment these preliminary experiments with MEMS stroke as a function of Kolmogorov atmosphere power.
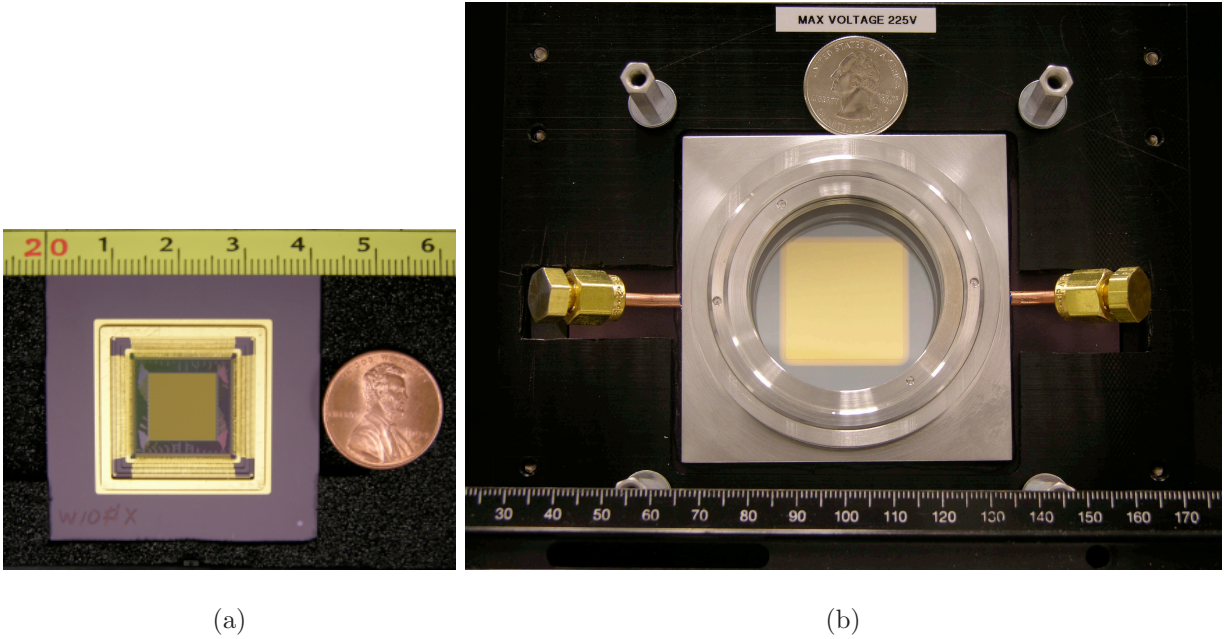
Figure 2. Boston Micromachines MEMS devices at the Laboratory for Adaptive Optics. (a) 1024-actuator DM with US penny and cm ruler. (b) 4096-actuator DM with US quarter and cm ruler. Note: These two mirrors are not to scale in relation to each other.
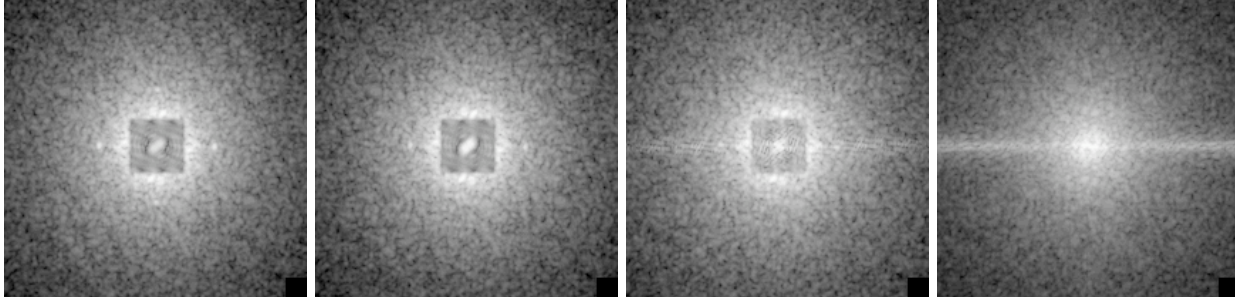

Figure 3. Effects of stroke saturation (which increases from left to right here) on the farfield image "dark hole". As stroke saturation increases, light scatters into the dark hole that is normally controlled by the MEMS. Any planets close to the central star would be undetectable. These plots are real data but not genuine farfield images: The MEMS was driven in closed-loop to a range of Kolmogorov atmosphere screens, and the residuals measured at the MEMS plane were made into the powerspectra seen here.

3. EXPERIMENTAL METHOD

Due to the nature of the dual-mirror architecture, it is possible to mitigate tweeter stroke saturation at spatial frequencies below the control-band of the woofer. Furthermore, if high-frequency saturation is found that can only be corrected by the MEMS, it is conceivable to make alternate tradeoffs in the engineering design of the device such as varying the mirror's surface thickness, which affects surface quality and maximum stroke. Therefore, it is necessary to test the MEMS for saturation incidence under conditions of Kolmogorov-atmosphere wavefront errors. We use our ExAO testbed with a phase-shifting diffraction interferometer[23] (PSDI) to explore this issue.

Because these experiments are conducted with a 1024-actuator MEMS in the LAO, rather than the 4096-actuator GPI MEMS, a decision has to be made to either keep the MEMS actuator pitch constant and reduce the size of the pupil, or to increase the size of the MEMS actuators with respect to the beam while maintaining the size of the pupil constant at 8m. In order to maintain and measure the effects of the high spatial frequencies,
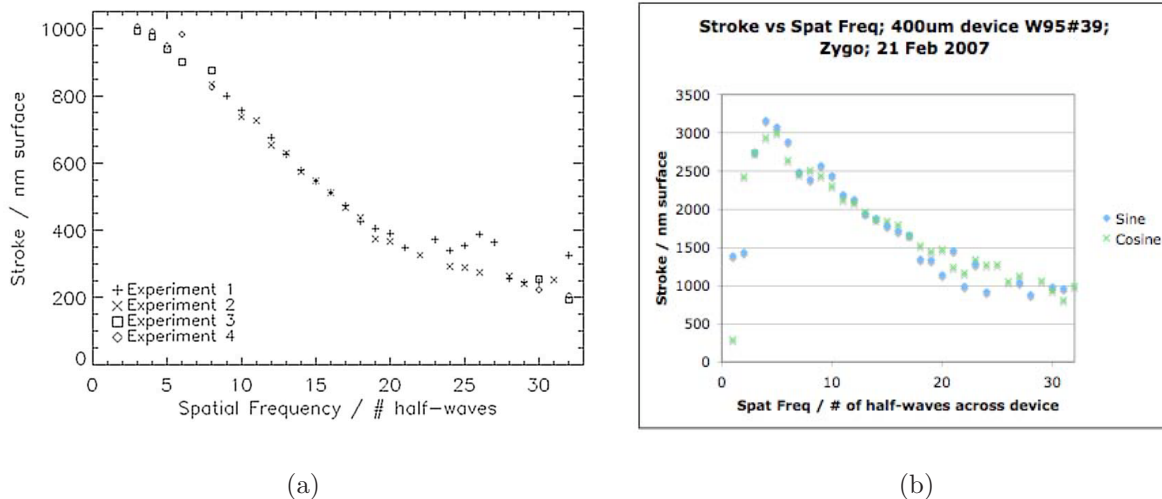
(a)   (b)

Figure 4. Stroke versus spatial frequency for (a) device "W10#X" with pitch 340 μm at voltage range 0-160V and (b) device "W95#39" with pitch 400 μm at voltage range 0-200V. Table 1 summarizes and contextualizes the results.

we choose to keep the MEMS actuator pitch with respect to the 8m-primary constant, thus decreasing the size of the pupil in the laboratory experiment to a $\sim$5m primary. Figure 5 shows the relative scaling of the MEMS actuators, the laboratory pupil, and the Gemini pupil used in the experiment. With the 1024-actuator MEMS used in the experiment, the primary pupil being tested is 4.9m in diameter.
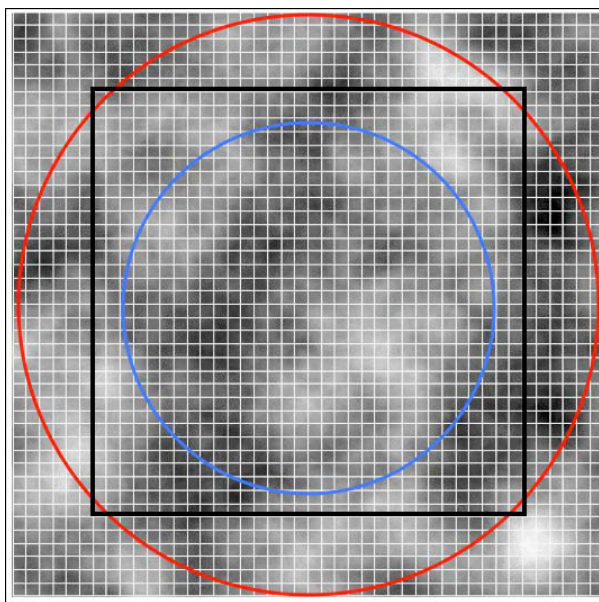
Figure 5. Relative scaling of the MEMS actuators, testbed pupil, and Gemini primary in the laboratory experiment. The fine white 44x44 grid represents MEMS actuators at GPI. The outer red circle represents the 8m Gemini primary. The inner black square delineates the 32x32 actuators of the 1024-MEMS used in the laboratory experiment. Finally, the inner blue circle represents the pupil of the ExAO testbed used in the experiment, which corresponds to a $\sim$5m primary. These shapes are superimposed on a scaled Kolmogorov atmosphere screen.

We produce software Kolmogorov atmospheres in IDL by creating a filter function and using it to generate random screens. To simulate the effects of a perfect woofer correction, we remove the low spatial frequencies by

truncating the filter below the woofer cutoff. The remaining higher frequencies are then applied to the MEMS in closed loop on the ExAO testbed in the LAO. Figure 6 illustrates the woofer application in one dimension, while Figure 7 shows the two-dimensional power spectra.
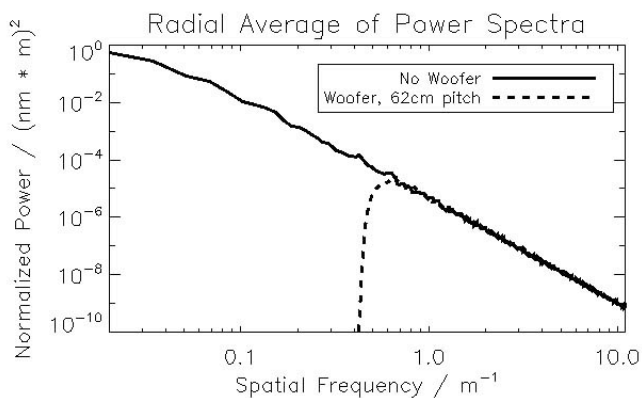

Figure 6. Radial averages of power spectra of Kolmogorov atmospheres. Solid line represents full Kolmogorov atmosphere at $r_0 = 10$ cm. Dashed line represents high frequencies that remain after 62 cm-pitch woofer is applied. All power lower than the woofer cutoff frequency is removed.

(a)   (b)
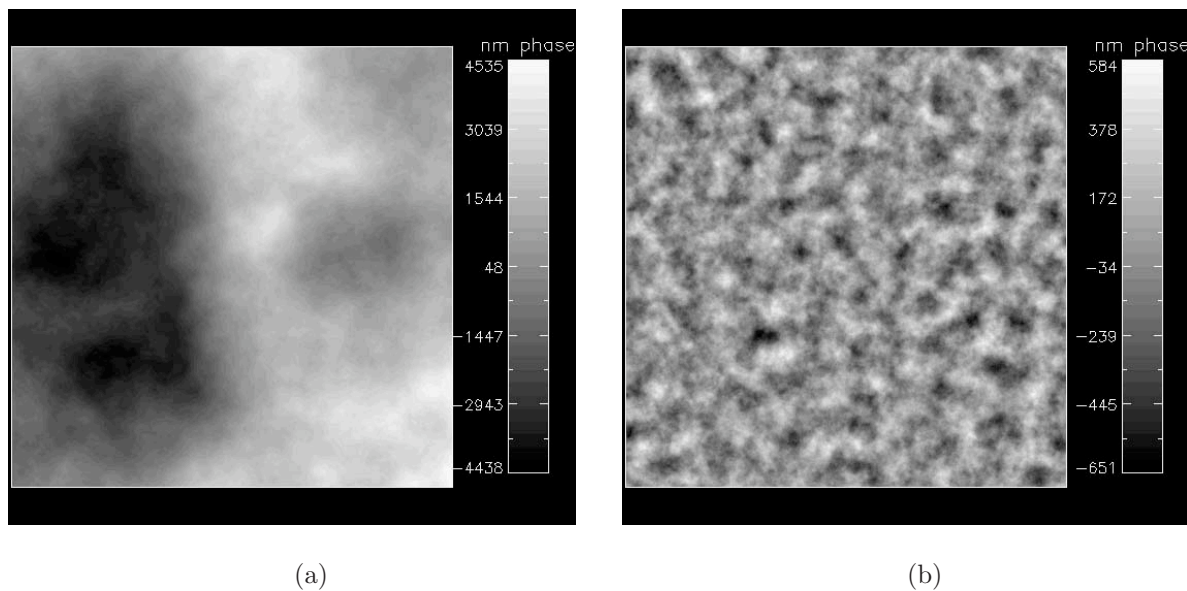
Figure 7. Power spectra of Kolmogorov atmospheres, $r_0 = 10$ cm. (a) Full Kolmogorov atmosphere screen—no woofer correction. (b) After 62 cm-pitch woofer correction, only high spatial frequencies remain. The woofer-removed screen is applied to the MEMS by driving to this shape in closed-loop.

After removing the lower spatial frequencies through software application of the woofer, the remaining high-frequency Kolmogorov atmosphere screen is applied to the MEMS by driving to the shape in closed-loop. The voltage range used is 0-200V. Figure 8 displays the resulting phase on the MEMS, resampled to 32x32 actuator spacing, as measured by the PSDI.
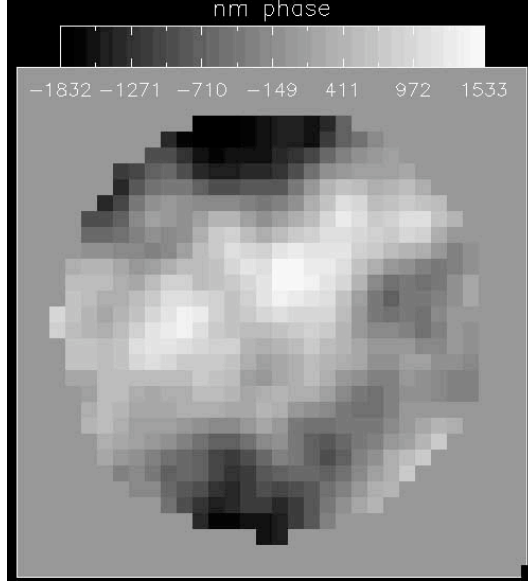
Figure 8. MEMS measurement, resampled to 32x32. On the ExAO testbed, the MEMS is driven in closed-loop to the input shape, a Kolmogorov atmosphere screen with some degree of woofer removal. The phase-shifting diffraction interferometer is used to measure the phase at the MEMS.

Woofer Pitch as Mapped onto Primary / cm	Number of Woofer Actuators across 5m Primary	Fraction of Actuators Saturated
No Woofer $\sim$ 490	1	$7.1 * 10^{-2}$
290	2	$4.3 * 10^{-2}$
134	4	$9.0 * 10^{-3}$
62	8	$5.4 * 10^{-3}$
40	12	$2.0 * 10^{-3}$
31	16	$7.1 * 10^{-4}$
MEMS — 18cm	*MEMS — 28 across 5m primary*	

Table 2. Table of woofer sizes varied with resulting actuator saturation fractions.

4. DATA AND RESULTS

We vary the woofer pitch from no woofer (which corresponds to about 490cm, or tip/tilt control only, as 4.9m is the size of the primary) to 31cm pitch at the primary, which is about 16 actuators across the primary. For comparison, the MEMS has an 18cm pitch when mapped to the primary, and there are 44 MEMS actuators across the GPI primary but only 28 actuators across the 5m primary in the testbed experiment. Table 2 lists the woofer sizes tried in the experiment and the number of saturated actuators found at each woofer size.

For each woofer pitch tried, the MEMS is driven to the shape in closed-loop. The gain is set low and the iterations high in order to approach the shape to the best ability of the MEMS. The PSDI is used to precisely measure the shape in closed-loop. After $\sim$20 iterations, the best shape (lowest rms residual) is saved and a different random iteration of the Kolmogorov atmosphere screen at $r_0 = 10\ cm$ is tried. At each woofer pitch, 10 to 50 different Kolmogorov atmosphere screens are applied to the MEMS.

The saturated actuators are found through the saved voltage data. As the voltage range used is 0-200V, any actuators at 0V in the best iteration are termed "saturated low" and any actuators at 200V are termed "saturated high." Figure 9 shows the voltages applied to the MEMS in the best iteration for four typical cases, for woofer pitches 500cm to 62cm. The saturated actuators are marked red or blue. The data shown are typical for each woofer case in the number of saturated actuators. The saturated actuators are distributed in clumps rather than as single saturated actuators. There is, as expected, a marked reduction in the quantity of saturated
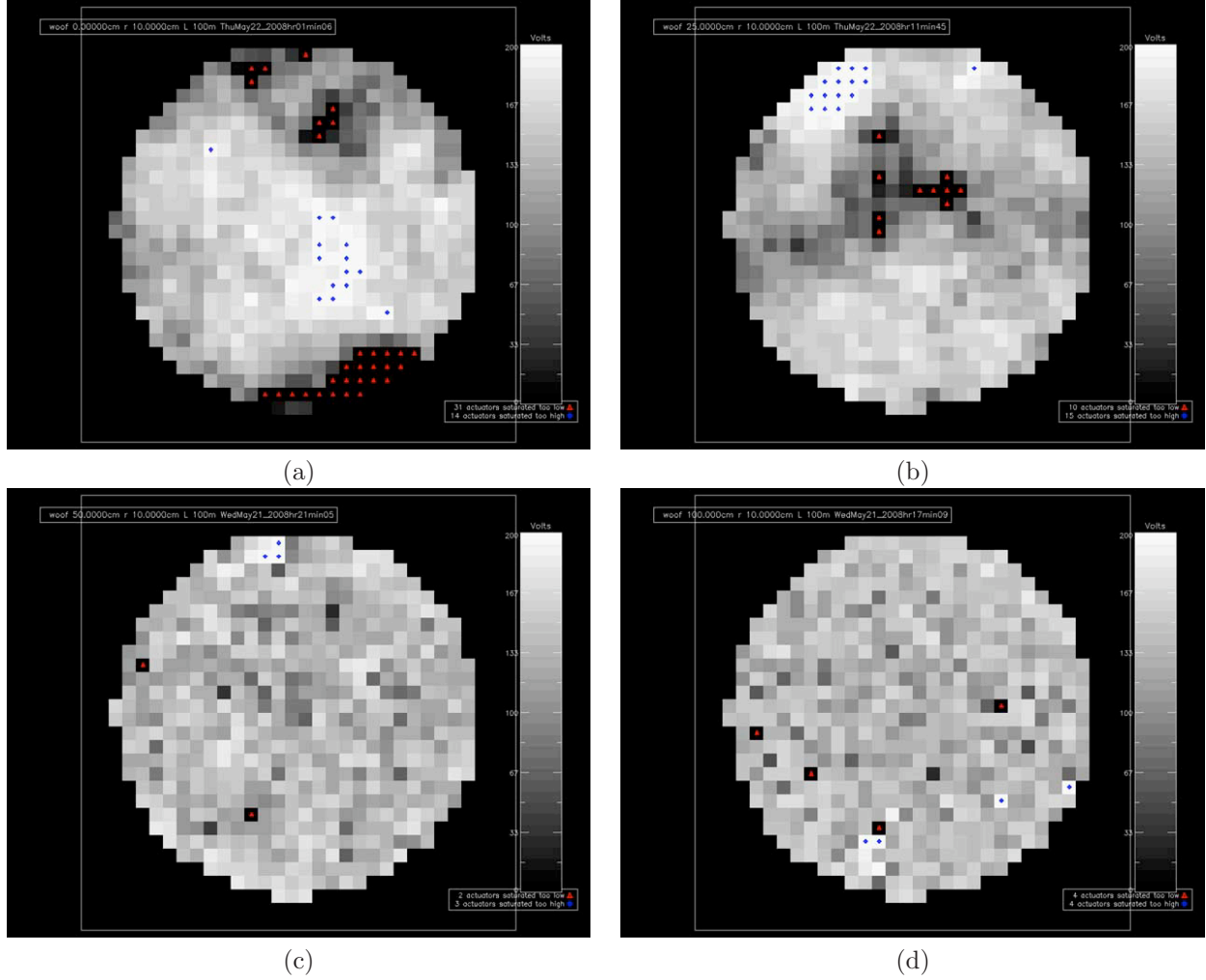
Figure 9. Maps of the voltages applied to the MEMS when closing to an $r_0 = 10\ cm$ software atmosphere. (a) No woofer ~ 490cm. (b) 290cm woofer. (c) 134cm woofer. (d) 62cm woofer. Red actuators are saturated low (0V) and blue actuators are saturated high (200V). Woofer pitch is given with respect to the primary pupil. Each case shown is typical in the number of actuators saturated at that woofer size. Note the clumpy distribution of saturated actuators and the decreasing saturation incidence with decreasing woofer-pitch; both features indicate that low-spatial-frequency phase aberrations in the atmosphere screens cause most of the saturation.

MEMS actuators as woofer pitch decreases. These trends indicate that the low-spatial-frequency aberrations are responsible for most of the saturation. The low spatial frequencies are controllable by a woofer, therefore this stroke saturation can be mitigated.

We also plot histograms (Figure 10) of the voltages applied to the MEMS in the best residual iteration. The first histogram shows the inter-actuator voltages applied. If a lot of neighboring actuator pairs are saturated, we would expect to see many inter-actuator voltages of close to 200V. Instead, there are almost no actuator pairs that are saturated at the high frequencies, for any woofer size. The trend with woofer size is to have a peakier distribution for larger woofer pitch, meaning more neighboring actuator pairs at lower gradients when the lower spatial frequencies are included. The second histogram shows the peak-to-valley difference voltages applied for each best residual. If the full range of the MEMS is being used, we expect to see a lot of the iterations at 200V difference. This is true for the cases with larger (or no) woofer actuators. Especially for the case with no woofer, almost 90% of the cases used the full voltage range and thus included some saturated actuators. However, as
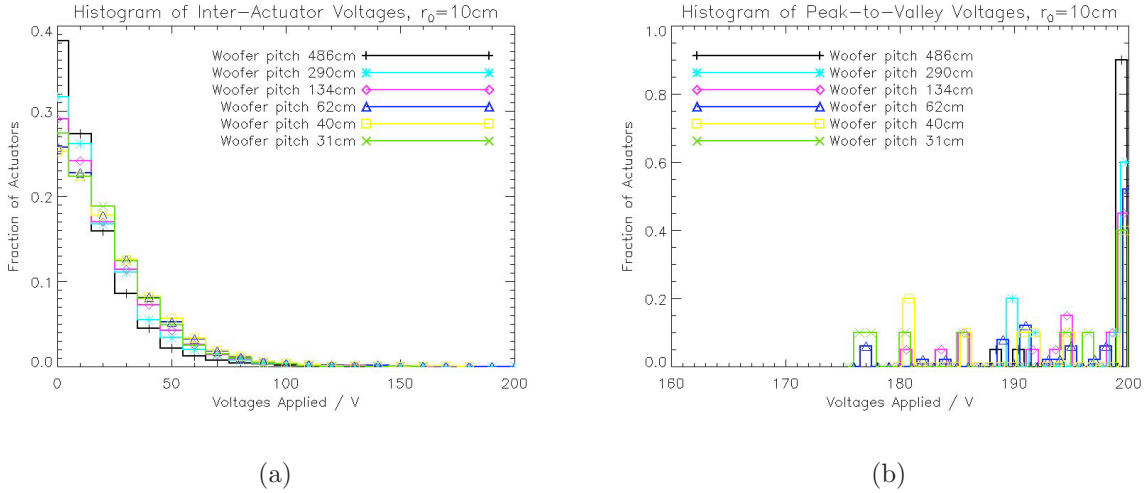
(a)   (b)

Figure 10. Histograms of voltage distribution applied to the MEMS to create the Kolmogorov atmosphere shape. (a) The histogram of inter-actuator voltages applied to the MEMS shows that very few neighboring actuator pairs were set to opposite extreme voltages (0-200V), at any woofer pitch. Therefore, there was very little high-spatial-frequency saturation. (b) The histogram of peak-to-valley voltages applied to the MEMS shows that, as woofer pitch decreases, the MEMS is increasingly able to deform to the atmospheric shape without using the full 0-200V range.

the woofer is introduced and its size decreased, the fraction of cases using the full voltage range drops to half for the 62cm woofer.

Finally, we plot the woofer size against fraction of actuators saturated (Figure 11). Reducing the woofer pitch as mapped to the primary gives fewer saturated MEMS actuators.

5. DISCUSSION

As seen in Figure 11, a 62cm woofer gives about a 3-sigma saturation chance. Recall that one of the GPI specification was 5 sigma saturation or less. There are several reasons why we are not yet worried. The experiment analyzed here was conducted for $r_0 = 10$ cm rather than the $r_0 = 15$ cm expected at Gemini South, in order to increase the signal received so that the saturated actuators could be well-counted in only 10 to 50 trials. The 1k-MEMS used has a physical pitch of 340 μm, but the GPI 4k-MEMS will have 400 μm and so will have more stroke (its goals are 4 μm peak-to-valley and 1.3 μm inter-actuator). Furthermore, the voltage range was 0-200V whereas the additional 60V (0-260V) we plan to operate for GPI may give a couple hundred nanometers more of stroke. Finally, the clumpily-distributed saturated actuators and the low incidence of saturated individual of neighboring actuator pairs indicates that a woofer will be successful in mitigating these low-spatial-frequency saturation events.

6. CONCLUSIONS

Saturation occurs primarily at lower spatial frequencies; therefore, peak-to-valley rather than inter-actuator stroke is the limiting factor. As woofer pitch decreases, saturation is mitigated to a few tenths of a percent and the full voltage range is not required as often. We measured ∼3-sigma saturation for ∼100cm-pitch woofer actuators at $r_0 = 10$ cm; future work is to vary r_0 in order to extrapolate this to the GPI 5-sigma tolerance, taking into consideration the fact that the base GPI 4k-MEMS has a larger pitch (400 μm) and will operate at

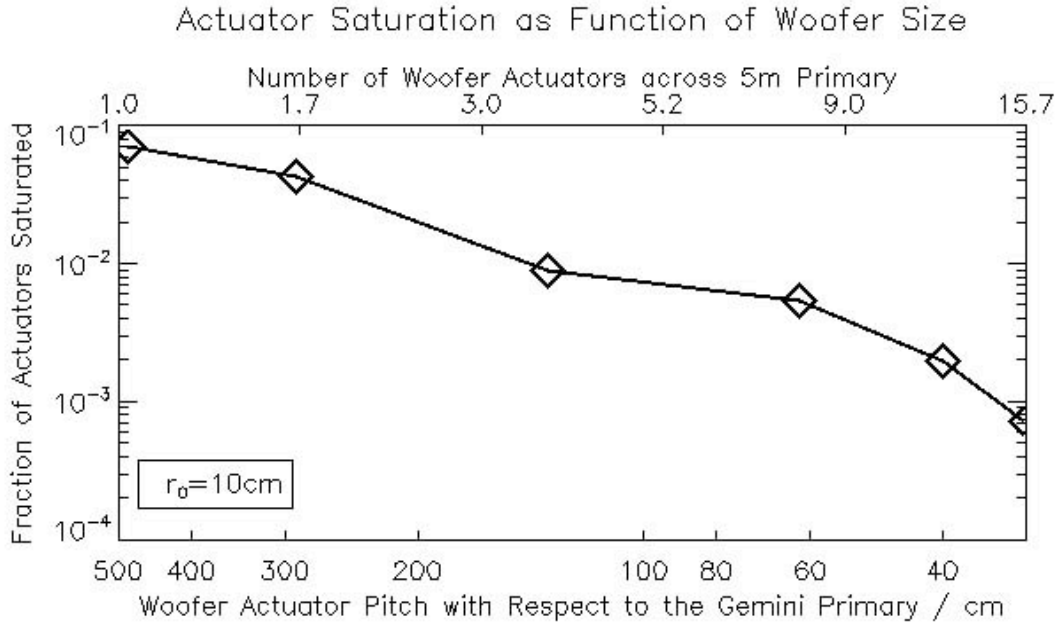## Actuator Saturation as Function of Woofer Size

Figure 11. Fraction of actuators saturated as a function of woofer size.

a wider voltage range (0-260 V). It will also be interesting to compare a stroke-versus-spatial-frequency curve from these measurements to the Kolmogorov power law.

ACKNOWLEDGMENTS

REFERENCES

1. P. Bodenheimer and D. N. C. Lin, "Implications of extrasolar planets for understanding planet formation," *Annu. Rev. Earth Planet. Sci.* **30**, pp. 113–148, 2002.

2. A. Wolszczan and D. A. Frail, "A planetary system around the millisecond pulsar psr1257 + 12," *Nature* **355**, pp. 145–147, 1992.

3. M. Mayor and D. Queloz, "A jupiter-mass companion to a solar-type star," *Nature* **378**, pp. 355–359, 1995.

4. A. Udalski, B. Paczynski, K. Zebrun, M. Szymanski, M. Kubiak, I. Soszynski, O. Szewczyk, L. Wyrzykowski, and G. Pietrzynski, "The Optical Gravitational Lensing Experiment. Search for Planetary and Low-Luminosity Object Transits in the Galactic Disk. Results of 2001 Campaign," *Acta Astronomica* **52**, pp. 1–37, Mar. 2002.

5. F. Bouchy, S. Udry, M. Mayor, C. Moutou, F. Pont, N. Iribarne, R. da Silva, S. Ilovaisky, D. Queloz, N. C. Santos, D. Ségransan, and S. Zucker, "ELODIE metallicity-biased search for transiting Hot Jupiters. II. A very hot Jupiter transiting the bright K star HD 189733," *A&A* **444**, pp. L15–L19, Dec. 2005.

6. I. A. Bond, A. Udalski, M. Jaroszyński, N. J. Rattenbury, B. Paczyński, I. Soszyński, L. Wyrzykowski, M. K. Szymański, M. Kubiak, O. Szewczyk, K. Żebruń, G. Pietrzyński, F. Abe, D. P. Bennett, S. Eguchi, Y. Furuta, J. B. Hearnshaw, K. Kamiya, P. M. Kilmartin, Y. Kurata, K. Masuda, Y. Matsubara, Y. Muraki, S. Noda, K. Okajima, T. Sako, T. Sekiguchi, D. J. Sullivan, T. Sumi, P. J. Tristram, T. Yanagisawa, and P. C. M. Yock, "OGLE 2003-BLG-235/MOA 2003-BLG-53: A Planetary Microlensing Event," *ApJL* **606**, pp. L155–L158, May 2004.

7. P. Kalas, "GPI: Gemini Planet Imager website," *http://gpi.berkeley.edu*, 2008.

8. B. Macintosh, J. Graham, D. Palmer, R. Doyon, D. Gavel, J. Larkin, B. Oppenheimer, L. Saddlemyer, J. K. Wallace, B. Bauman, J. Evans, D. Erikson, K. Morzinski, D. Phillion, L. Poyneer, A. Sivaramakrishnan, R. Soummer, S. Thibault, and J.-P. Veran, "The Gemini Planet Imager," in *Advances in Adaptive Optics II*, B. L. Ellerbroek and D. B. Calia, eds., *Proc. SPIE* **6272**, p. 62720L, 2006.

9. B. Macintosh, J. Graham, D. Palmer, R. Doyon, J. Dunn, D. Gavel, J. Larkin, B. Oppenheimer, L. Saddlemyer, A. Sivaramakrishnan, J. K. Wallace, B. Bauman, D. Erikson, C. Marois, L. Poyneer, and R. Soummer, "The Gemini Planet Imager: From science to design to construction," in *Adaptive Optics Systems*, N. Hubin, C. E. Max, and P. L. Wizinowich, eds., *Proc. SPIE* **7015**, p. 701543, 2008.

10. T. Bifano, P. Bierden, and J. Perreault, "Micromachined deformable mirrors for dynamic wavefront control," in *Advanced Wavefront Control: Methods, Devices and Applications II*, J. D. Gonglewski, M. T. Gruineisen, and M. K. Giles, eds., *Proc. SPIE* **5553**, pp. 1–16, 2004.

11. P. J. Hampton, R. Conan, C. Bradley, and P. Agathoklis, "Control of a woofer tweeter system of deformable mirrors," in *Advanced Software and Control for Astronomy*, H. Lewis and A. Bridger, eds., *Proc. SPIE* **6274**, p. 62741Z, 2006.

12. J. W. Evans, G. Sommargren, L. Poyneer, B. Macintosh, S. Severson, D. Dillon, A. Shenis, D. Palmer, J. Kasdin, and S. Olivier, "Extreme adaptive optics testbed: Results and future work," in *Advancements in Adaptive Optics*, D. B. Calia, B. L. Ellerbroek, and R. Ragazzoni, eds., *Proc. SPIE* **5490**, pp. 954–959, 2004.

13. J. W. Evans, K. Morzinski, L. Reza, S. Severson, L. Poyneer, B. Macintosh, D. Dillon, G. Sommargren, D. Palmer, D. Gavel, and S. Olivier, "Extreme adaptive optics testbed: High contrast measurements with a MEMS deformable mirror," in *Techniques and Instrumentation for Detection of Exoplanets II*, D. R. Coulter, ed., *Proc. SPIE* **5905**, pp. 303–310, 2005.

14. J. W. Evans, B. Macintosh, L. Poyneer, K. Morzinski, S. Severson, D. Dillon, D. Gavel, and L. Reza, "Demonstrating sub-nm closed loop MEMS flattening," *Optics Express* **14**, pp. 5558–5570, 2006.

15. J. W. Evans, G. Sommargren, B. A. Macintosh, S. Severson, and D. Dillon, "Effect of wavefront error on 10^{-7} contrast measurements," *Optics Letters* **31**, pp. 565–567, 2006.

16. D. Gavel, "MEMS development for astronomical instrumentation at the Lick Observatory Laboratory for Adaptive Optics," in *MEMS Adaptive Optics*, S. S. Olivier, T. G. Bifano, and J. A. Kubby, eds., *Proc. SPIE* **6467**, p. 646702, 2007.

17. D. T. Gavel, S. A. Severson, B. J. Bauman, D. R. Dillon, M. R. Reinig, C. Lockwood, D. W. Palmer, K. M. Morzinski, S. M. Ammons, E. L. Gates, and B. Grigsby, "Villages: An on-sky visible wavelength astronomy AO experiment using a MEMS deformable mirror," in *MEMS Adaptive Optics II*, S. S. Olivier, T. G. Bifano, and J. A. Kubby, eds., *Proc. SPIE* **6888**, p. this conference, 2008.

18. K. M. Morzinski, J. W. Evans, S. Severson, B. Macintosh, D. Dillon, D. Gavel, C. Max, and D. Palmer, "Characterizing the potential of MEMS deformable mirrors for astronomical adaptive optics," in *Advances in Adaptive Optics II*, B. L. Ellerbroek and D. B. Calia, eds., *Proc. SPIE* **6272**, p. 627221, 2006.

19. K. M. Morzinski, K. B. W. Harpsøe, D. Gavel, and S. M. Ammons, "The open-loop control of MEMS: Modeling and experimental results," in *MEMS Adaptive Optics*, S. Olivier, T. G. Bifano, and J. A. Kubby, eds., *Proc. SPIE* **6467**, p. 64670G, 2007.

20. K. M. Morzinski, D. Gavel, A. Norton, D. Dillon, and M. Reinig, "Characterizing MEMS deformable mirrors for open-loop operation: High-resolution measurements of thin-plate behavior," in *MEMS Adaptive Optics II*, S. S. Olivier, T. G. Bifano, and J. A. Kubby, eds., *Proc. SPIE* **6888**, p. 68880S, 2008.

21. S. A. Severson, B. Bauman, D. Dillon, J. Evans, D. Gavel, B. Macintosh, K. Morzinski, D. Palmer, and L. Poyneer, "The Extreme Adaptive Optics Testbed at UCSC: Current results and coronagraphic upgrade," in *Advances in Adaptive Optics II*, B. L. Ellerbroek and D. B. Calia, eds., *Proc. SPIE* **6272**, p. 62722J, 2006.

22. J.-F. Lavigne and J.-P. Veran, "Woofer-tweeter control in adaptive optics system using a Fourier reconstructor," *JOSA* , in press.

23. G. E. Sommargren, D. W. Phillion, M. A. Johnson, N. Q. Nguyen, A. Barty, F. J. Snell, D. R. Dillon, and L. S. Bradsher, "100-picometer interferometry for EUVL," in *Emerging Lithographic Technologies VI*, R. L. Engelstad, ed., *Proc. SPIE* **4688**, pp. 316–328, 2002.